remote sensing

MDPI

Article

A Framework for Satellite-Based 3D Cloud Data: An Overview of the VIIRS Cloud Base Height Retrieval and User Engagement for Aviation Applications

Yoo-Jeong Noh [1,*], John M. Haynes [1], Steven D. Miller [1], Curtis J. Seaman [1], Andrew K. Heidinger [2], Jeffrey Weinrich [3], Mark S. Kulie [2], Mattie Niznik [1] and Brandon J. Daub [1]

[1] Cooperative Institute for Research in the Atmosphere, Colorado State University, Fort Collins, CO 80523, USA
[2] National Oceanic and Atmospheric Administration, National Environmental Satellite, Data, and Information Service, Madison, WI 53706, USA
[3] National Oceanic and Atmospheric Administration, National Weather Service, Office of Science and Technology Integration, Silver Springs, MD 20910, USA
* Correspondence: yoo-jeong.noh@colostate.edu

Abstract: Satellites have provided decades of valuable cloud observations, but the data from conventional passive radiometers are biased toward information from at or near cloud top. Tied with the Joint Polar Satellite System (JPSS) Visible Infrared Imaging Radiometer Suite (VIIRS) Cloud Calibration/Validation research, we developed a statistical Cloud Base Height (CBH) algorithm using the National Aeronautics and Space Administration (NASA) A-Train satellite data. This retrieval, which is currently part of the National Oceanic and Atmospheric Administration (NOAA) Enterprise Cloud Algorithms, provides key information needed to display clouds in a manner that goes beyond the typical top-down plan view. The goal of this study is to provide users with high-quality three-dimensional (3D) cloud structure information which can maximize the benefits and performance of JPSS cloud products. In support of the JPSS Proving Ground Aviation Initiative, we introduced Cloud Vertical Cross-sections (CVCs) along flight routes over Alaska where satellite data are extremely helpful in filling significant observational gaps. Valuable feedback and insights from interactions with aviation users allowed us to explore a new approach to provide satellite-based 3D cloud data. The CVC is obtained from multiple cloud retrieval products with supplementary data such as temperatures, Pilot Reports (PIREPs), and terrain information. We continue to improve the product demonstrations based on user feedback, extending the domain to the contiguous United States with the addition of the Geostationary Operational Environmental Satellite (GOES)-16 Advanced Baseline Imager (ABI). Concurrently, we have refined the underlying science algorithms for improved nighttime and multilayered cloud retrievals by utilizing Day/Night Band (DNB) data and exploring machine learning approaches. The products are evaluated using multiple satellite data sources and surface measurements. This paper presents our accomplishments and continuing efforts in both scientific and user-engagement improvements since the beginning of the VIIRS era.

Keywords: VIIRS; cloud base height retrieval; 3D satellite cloud products; aviation weather applications; user engagement

Citation: Noh, Y.-J.; Haynes, J.M.; Miller, S.D.; Seaman, C.J.; Heidinger, A.K.; Weinrich, J.; Kulie, M.S.; Niznik, M.; Daub, B.J. A Framework for Satellite-Based 3D Cloud Data: An Overview of the VIIRS Cloud Base Height Retrieval and User Engagement for Aviation Applications. *Remote Sens.* **2022**, *14*, 5524. https://doi.org/10.3390/rs14215524

Academic Editor: Alexander Marshak

Received: 27 August 2022
Accepted: 1 November 2022
Published: 2 November 2022

1. Introduction

Clouds are one of the most uncertain factors in global climate modeling and play an important role in weather forecasting as visible indicators of hazardous weather conditions. A better understanding and more accurate parameterizations of clouds are critical to advancing various weather applications used operationally for hazardous condition forecasting [1,2] and climate studies related to global radiative impacts [3–6]. Comprehensive cloud information is particularly critical in data-sparse regions such as Alaska where weather conditions can change rapidly and many residents rely on aviation to access

goods and services. More reliable cloud data that aviation meteorologists and pilots can practically utilize and readily assess for weather conditions are required to make safe flight decisions, thus supporting aviation safety [7,8].

Satellite-derived cloud products provide crucial information about global cloud properties. In the realm of polar-orbiting satellites, the Advanced Very High Resolution Radiometer (AVHRR) sensors carried on the U. S. NOAA polar-orbiting platforms (POES) and the European Organisation for the Exploitation of Meteorological Satellites (EUMETSAT) [Meteorological Operational (MetOp)] satellites with morning and afternoon acquisitions have offered long-term cloud data since 1978 [9,10]. In particular, observations provided by the Moderate Resolution Imaging Spectroradiometer (MODIS) [11] on board the National Aeronautics and Space Administration (NASA) Terra and Aqua satellites contributed significantly to advancing our understanding and retrieval techniques on cloud distributions and microphysical properties with higher spectral resolution [12]. More recently, observations from the VIIRS instrument aboard two Joint Polar Satellite System (JPSS) satellites, the NOAA/NASA Suomi National Polar-orbiting Partnership (Suomi NPP or S-NPP) and NOAA-20, have been providing useful cloud information, ensuring the continuity of meteorological observations from polar orbit.

Leveraging the technical and scientific advances from these polar-orbiting satellites, the next-generation geostationary satellites such as the Japanese Himawari-8 Advanced Himawari Imager (AHI) [13], U.S. NOAA GOES-R series carrying the ABI [14], the Chinese Feng Yun-4 series (FY-4) with the Advanced Geosynchronous Radiation Imager (AGRI) [15], and the South Korean GEOstationary Korea Multi-Purpose SATellite-2A (GEO-KOMPSAT-2A or GK-2A) with the Advanced Meteorological Imager (AMI) [16] have provided global cloud observations with significantly advanced temporal/spatial resolutions equipped with 14–16 spectral bands in the visible, near-IR, and IR spectrum.

Satellite remote sensing via these conventional passive radiometers such as VIIRS and ABI has provided a ready means of estimating various cloud properties, including cloud top height, optical thickness (COT), and effective particle size (EPS) [17–19]. However, the information from these sensors using passive radiometers is limited mostly to 2D cloud-top views, which lack information about vertical cloud structure. The ability to probe deeper into clouds and describe their vertical structure is challenging due to the inherent limited sensitivity of passive radiometers to this information—while instead providing bulk information on the vertically integrated properties.

Cloud base height (CBH; referred to as "cloud ceiling" when pertaining to the cloud layer closest to the surface) is a crucial parameter for weather and climate research, including aviation weather applications [7,20–23]. For example, knowledge of CBH relative to the 0° Celsius isotherm is of prime importance to identifying the vertical extent of potential aircraft icing hazards as well as pilot visibility, e.g., [24,25], since cloud particles can exist in liquid phase at sub-freezing temperatures depending on the composition of the aerosol environment in which they formed. CBH and related parameters such as cloud base temperature and pressure directly impact downwelling longwave radiative fluxes, and thus alter global radiative balance and climate [26–29].

Several methods for satellite-based CBH retrieval have been attempted to confront this challenge using different sensors over the last few decades. Passive microwave measurements have been used for cloud vertical information, e.g., [30,31]. Wilheit and Hutchison [32] proposed a CBH retrieval method by combining passive microwave brightness temperature and infrared (IR) cloud top temperature data. Light scattering characteristics inside and below the cloud in the oxygen A-band have been utilized in estimating cloud geometric thickness (CGT) which can be used to infer CBH [33–36]. A spectral radiance matching algorithm that combines CBH observations from active radar and lidar sensors with passive visible (VIS) and IR imagery has been investigated [37,38]. A combination of cloud retrieval products and ancillary data has been employed to derive CBH for cloudy pixels for VIS and IR passive sensors, e.g., [39–41].

A few data fusion methods have also been explored combining satellite VIS and IR data with surface-based observations, e.g., [7,24,42]. A data mining algorithm has been used to relate VIS and IR satellite imagery with numerical weather prediction (NWP) model data for cloud ceilings [43]. An assumption of adiabatic processes is often used to derive cloud thickness for boundary layer clouds [44–46]. More recently, machine learning approaches have been employed to estimate CBHs, e.g., [47,48].

Among these approaches, the CBH retrieval method based on Hutchison et al.'s studies [39,40] was selected as one of the S-NPP VIIRS operational Environmental Data Records (EDRs) produced through the Interface Data Processing Segment (IDPS), which was the original ground system developed by the JPSS program to distribute JPSS data products. We refer to this initial version of VIIRS CBH as IDPS CBH. However, previous research using CloudSat data showed that IDPS CBH errors exceeded the JPSS program error specifications [49]. This validation study led to the development of a new statistical CBH algorithm with improved performance meeting the JPSS specifications [50], which is now part of the NOAA Enterprise Cloud Algorithms. The full list of VIIRS cloud products can be found at https://www.star.nesdis.noaa.gov/jpss/clouds.php (accessed on 31 October 2022).

This paper presents our research efforts to provide users with improved 3D cloud structure information increasing the utility of JPSS cloud products. We developed a statistical CBH algorithm, tied with JPSS Cloud Calibration/Validation activities started with the VIIRS launch in 2011, which is a key component for 3D cloud data. The algorithm is currently operational for JPSS VIIRS and is also used to improve the ABI Cloud Cover Layers (CCL) products onboard the GOES-R series of satellites. In particular, using the CBH information together with multiple cloud retrieval products, we introduce an innovative approach to build 3D cloud structures. This development allows pilots to anticipate cloud conditions in three dimensions along a vertical path within a cloud cross-section. The approach has been improved through active interactions with aviation users. These important user-engagement activities are addressed together with current scientific approaches for further refinements of the algorithm and products.

The paper is structured as follows: Section 2 reviews the physical basis and construction of the CBH algorithm; Section 3 presents validation of the algorithm; Section 4 details the application of the CBH information to an improved version of the CCL product; Section 5 describes efforts to extend the 3D cloud structure description to multi-layer profiles via machine-learning and model-fusion techniques; Section 6 examines the utility of these products in the context of aviation user; Section 7 considers the specific challenges and algorithm modifications necessary to enable 3D cloud estimates at night; and Section 8 concludes the paper.

2. An Overview of the CBH Algorithm

Retrieval of CGT provides the information needed to convert 2D cloud information into a first-order estimate of 3D cloud structure. Cloud information from visible, shortwave infrared (SWIR), and thermal infrared (TIR) satellite instruments such as VIIRS is mostly biased toward the cloud top due to natural limitations of the wavelengths available with traditional passive radiometers; in a cloudy atmosphere, the spectral characteristics of these wavelengths result in the observation of radiation that is primarily reflected or emitted from near cloud tops, but there is limited information about radiation originating from deeper inside cloud layers. While infrared channels can estimate cloud top height (CTH), and visible/SWIR information provides an estimate of vertically integrated water content (Cloud Water Path; CWP), they cannot measure CBH directly.

The IDPS CBH was the original operational algorithm to retrieve CBH from VIIRS. Through validation studies tied to the JPSS program, IDPS CBH products for S-NPP were compared against CloudSat observations, which provide highly vertically resolved cloud boundaries from a spaceborne 94-GHz nadir-looking radar. Since S-NPP and CloudSat flew in the same orbital plane for several years, but at different altitudes (834 km and 705 km, respectively), these instruments provide nearly simultaneous observations of the

same locations on Earth for a 4.5-h period every 2–3 days. The details of the evaluation methodology by which VIIRS and CloudSat observations are spatially and temporally matched are outlined in Seaman et al. [49]. We found that the performance of the IDPS CBH algorithm was impacted by the accuracy of upstream retrievals (such as CTH and the cloud type which was used to prescribe a characteristic cloud water content) and the a priori information used by the CBH retrieval algorithm. With these limitations in play, the initial IDPS CBH provided only marginal skill. These performance shortfalls, and ensuing discussions of canceling production of the CBH product prompted exploration of alternative approaches to the initial IDPS CBH algorithm.

To this end, a statistical CBH algorithm was developed using global passive-active sensor cloud observations from NASA A-Train satellites: Aqua MODIS, CloudSat radar, and Cloud-Aerosol Lidar and Infrared Pathfinder Satellite Observation (CALIPSO) lidar [18,51–54]. The notion of statistically relating observed CGT to various cloud properties using space-borne active sensor data from CloudSat and CALIPSO, done not as an explicit and discrete function of cloud type but instead as an implicit and continuous relationship, was built on the work of Miller et al. [22]. The active sensor data sets have been used to retrieve quantitative cloud properties such as ice/liquid water contents and precipitation [55–57]; in this case, they were used as a form of training (and validation) for the CGT estimates. Here, we provide a brief description of the retrieval, with a full description found in Noh et al. [50].

The statistical semi-empirical approach for retrieving CBH from VIIRS is readily extendable to other similar passive visible and IR satellite observations. This CBH algorithm is constrained by CTH and CWP, with supplementary NWP data, and using statistical analyses of NASA A-Train satellites data (global July data from 2007–2010). To build the algorithm, Aqua MODIS provided cloud cover, cloud top height, and cloud water path information across a 2330 km swath. CloudSat and CALIPSO data were used to identify vertical cloud geometric boundaries as shown in Figure 1.

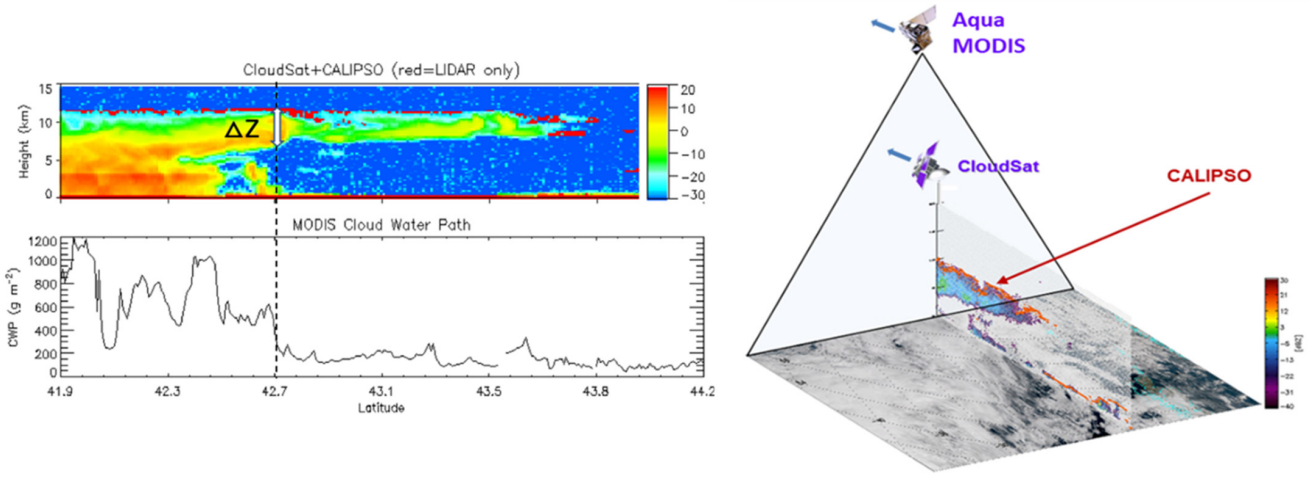

Figure 1. Sample of space-borne active-passive sensor data combinations for the CBH algorithm development using A-Train satellite data (Aqua MODIS and CloudSat/CALIPSO).

With this information, we derived a statistical relationship between CWP and CGT constrained by CTH, yielding a set of pre-established, global statistical relationships, described in detail by Noh et al. [50]. The CBH is derived by subtracting the estimate of CGT from the retrieved CTH. Additional provisions were made for particularly challenging cloud types, applying an extinction-based method for thin cirrus (COT < 1) which was developed using CALIPSO data, and employing NWP-derived convective and lifting condensation level data to assign CBH in cases of deep convection. Figure 2 shows a flowchart of the algorithm (adapted from [50]).

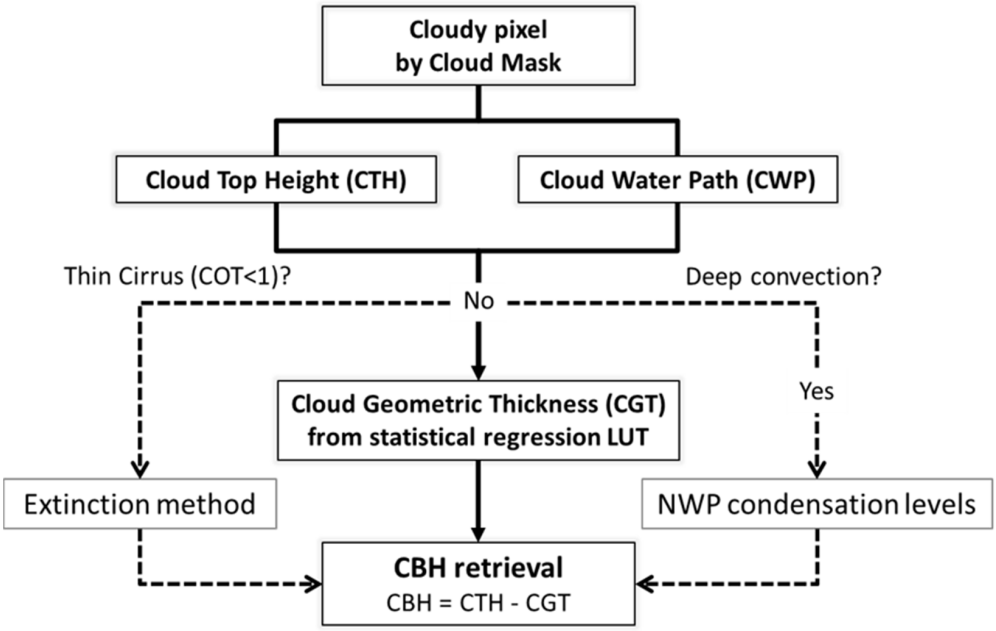

Figure 2. A schematic diagram of the statistical CBH algorithm for single-layer clouds (modified from Noh et al. [50]).

The accuracy of CTH and CWP used as input for the CBH algorithm is important as it relates directly to uncertainties in the CBH output. It is also noted that nighttime collection requires using additional data from NWP models, since the quality of the CWP retrievals is degraded compared to daytime products due to lack of visible information used in multiple upstream cloud retrievals, including the cloud mask and cloud optical thickness. Further, the CBH algorithm targets the uppermost cloud layer; it performs best on single-layer clouds and can be considered a 'ceiling,' but may show marginal skill in complex, multi-layer cloud scenes.

The algorithm has been applied to S-NPP/NOAA-20 VIIRS and evaluated against independent CloudSat and CALIPSO data. This statistical CBH algorithm outperformed the IDPS CBH and is now operational as part of the NOAA Enterprise Cloud algorithms. The Algorithm Theoretical Basis Document (ATBD) is available at https://www.star.nesdis.noaa.gov/jpss/clouds.php and VIIRS official products from S-NPP and NOAA-20 satellites are publicly available at the NOAA Comprehensive Large Array-data Stewardship System (CLASS; https://www.class.noaa.gov). For general users, the CBH and CCL products are also displayed in near real-time at CIRA's VIIRS Arctic website with an archive for Alaska (http://rammb.cira.colostate.edu/ramsdis/online/npp_viirs_arctic.asp (accessed on 31 October 2022)).

These cloud products and other VIIRS imagery for polar regions can also be viewed on the CIRA Satellite Loop Interactive Data Explorer in Real-time (SLIDER; [58]) website (https://rammb-slider.cira.colostate.edu). SLIDER displays real-time satellite imagery for the polar environment, including flight level-based cloud layers on a loop. Sample composites are shown in Figure 3. VIIRS Cloud Phase in these websites also includes the "Supercooled Liquid-Topped Mixed-Phase (LTMP)" category for lower-level cloud phase information under the cloud top [5,59].

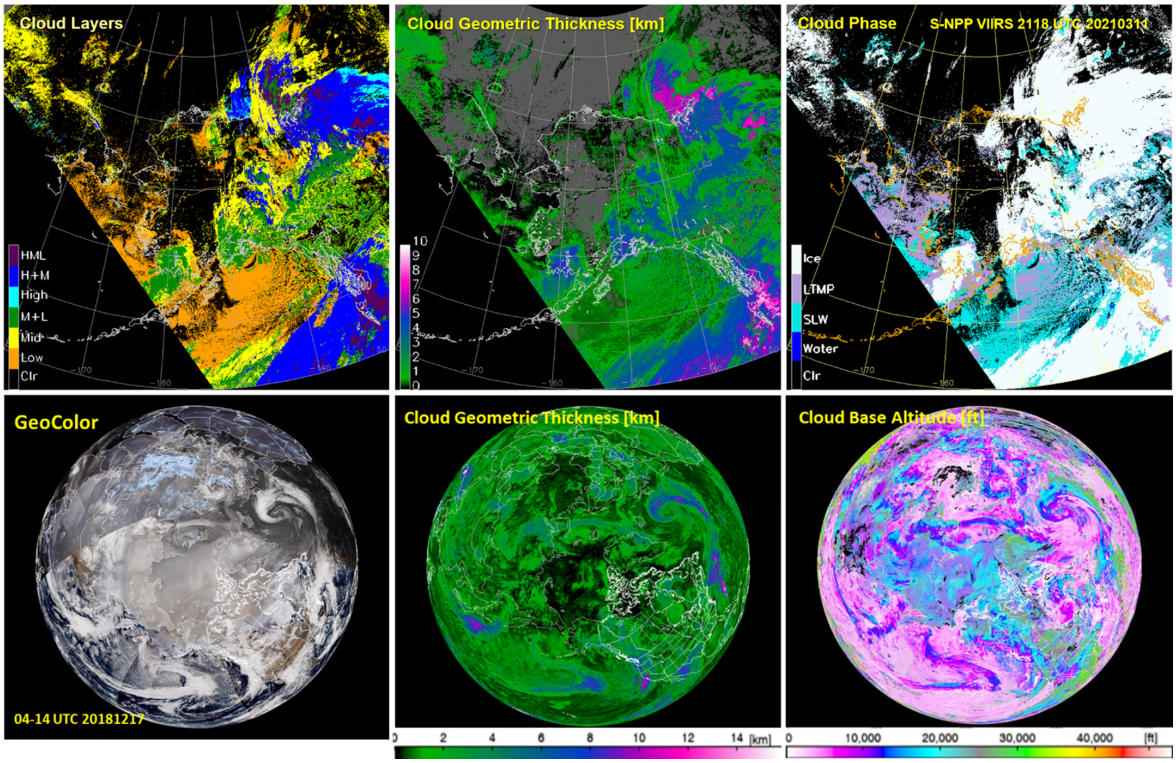

Figure 3. VIIRS cloud product examples. The upper panels show Cloud Layers, Cloud Geometric Thickness (CGT), and Cloud Phase imagery over Alaska (**upper panels**). The **bottom panels** show global CGT and Cloud Base Altitude (in feet for aviation users) together with VIIRS GeoColor over the Northern Hemisphere as displayed on CIRA's SLIDER website.

3. Validation

Product evaluation is a critical yet challenging activity for CBH and CCL products due to limited suitable observational data. Using available data resources, the products have been validated against surface-based and space-based observations for the purpose of further refinements and long-term monitoring. Through multi-month matchup evaluations between VIIRS and CloudSat, we confirmed that the new Enterprise CBH algorithm performs better than the IDPS CBHs. Table 1 summarizes error statistics of the new algorithm (Enterprise) and IDPS CBHs previously examined for September-October 2013 matchups and January-May 2015 matchups between S-NPP VIIRS and CloudSat [50]. Figure 4 shows the September-October 2013 matchups of IDPS and the Enterprise CBHs against CloudSat data for all cloud types (top panels), and also includes new comparisons which were additionally conducted for the Enterprise CBHs for two specific cloud categories: (1) optically thin clouds (COT < 1), and (2) low liquid water clouds (which CALIPSO can detect better than CloudSat).

Table 1. Error statistics of the new algorithm and IDPS CHBs from S- NPP VIIRS–CloudSat matchups (Modified from Noh et al. [50]).

CBHs (km) within Spec Only	Average Error (Bias)	RMSE	r^2
September–October 2013 matchups			
Enterprise (95,145)	0.3	1.7	0.79
IDPS (85,495)	0.7	2.7	0.45
January–May 2015 matchups			
Enterprise (216,745)	0.4	1.7	0.80
IDPS (162,079)	1.3	2.7	0.49

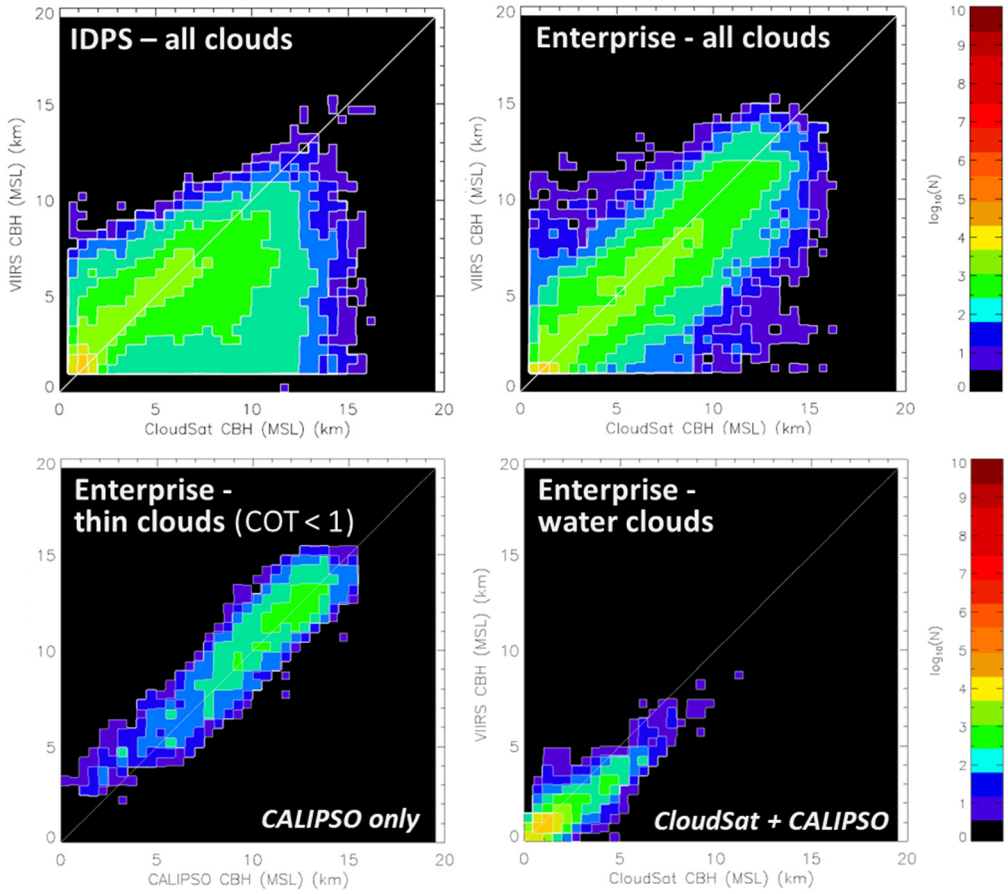

Figure 4. An example of comparisons with independent CloudSat radar and CALIPSO lidar data (modified from Noh et al. 2017). "Within-spec" two-dimensional histograms of VIIRS-retrieved and CloudSat-observed CBH for the original IDPS CBH algorithm with CLAVR-x input (**upper left**), and (**right**) the statistical Enterprise algorithm (implemented in the CLAVR-x system) for September–October 2013. The bottom panels show optically thin clouds from the Enterprise CBH algorithm compared with CALIPSO lidar data and water clouds compared with CloudSat and CALIPSO combined data, respectively. Colors represent the number of data points (N; shown on a logarithmic scale). The comparisons are valid for all cloud types encountered globally.

Another way to validate satellite information is to compare this data against ground-based measurements such as those of the Atmospheric Radiation Measurement (ARM) program, sponsored by the U.S. Department of Energy (DOE). We use ceilometer and micro-pulse lidar measurements from the ARM sites on the Northern Slope of Alaska (NSA in Alaska) and the Southern Great Plains (SGP in Oklahoma). Figure 5 shows a three-year comparison between VIIRS CBH estimates and ARM ground observations from ceilometers (black and gray) and micro-pulse lidar (red and brown). Multi-layer clouds can cause outliers, which are particularly notable in the SGP area, possibly having more complex cloud cases. Nighttime CBHs from nighttime cloud properties (Nighttime Lunar Cloud Optical and Microphysical Algorithm-NLCOMP using DNB) are colored in blue.

In all, we evaluated three years of ARM data at both the NSA (2285 matchups) and SGP sites (745 matchups) to determine what percentage of cloud base observations occurred within a 2 km vertical window of the corresponding CBH observation from S-NPP and NOAA-20. For the NSA site, these percentages were 89.23% for ceilometer data and 82.10% for MPL measurements; for the SGP site, they were 85.10% for ceilometer data and 67.79% for MPL data. It is noted that "Within-spec" data mean when VIIRS CTH is within 2 km of the surface lidar-derived CTH (offering a valid comparison). This within-spec comparison can help eliminate large CTH disagreement which is inherited from the upstream retrieval

as an additional source of CBH errors. Precipitation cases were excluded in the evaluation using ARM MET data. Collocations between VIIRS (parallax-corrected) and ARM locations were performed within 0.1° and 5-min windows.

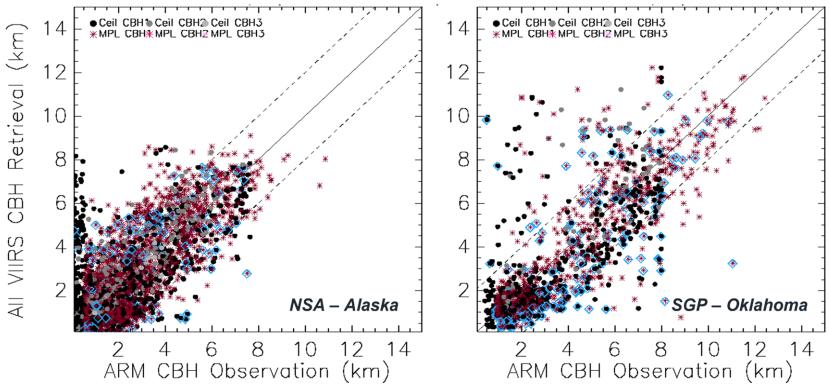

Figure 5. CBH comparisons of VIIRS and ground-based data from Ceilometer (black and gray for layers) and Micro-Pulse Lidar (red and brown) collected from an Atmospheric Radiation Measurement (ARM) Alaska NSA site (**left**; 2285 cases) and Oklahoma SGP site (**right**: 770 cases) for 2019–2021. Note that matchups are valid only when CTH from lidar (MPL) is within a 2 km accuracy range compared with VIIRS CTH ("within-spec"). Dotted lines represent 2 km error ranges, and CBHs from a nighttime cloud optical property algorithm (NLCOMP) using DNB are colored in blue.

CALIPSO data having near-simultaneous colocation with these surface observations have been added to capture multi-layered cloud cases which have optically thin (COT < 1) clouds aloft for selected case studies (Figure 6). The Multi-Radar/Multi-Sensor System (MRMS) data, which is an operational data integration system including a network of radars, surface and upper-air observations, lightning detection systems, satellite, and forecast models [2,60], is also available on CIRA's SLIDER website and offers instantaneous qualitative comparisons of the products. PIREPs can provide additional information for cloud phase-related icing potential assessment. Since the algorithms are also applicable to other sensors such as ABI and AHI onboard geostationary satellites, the inter-comparisons of the products offer opportunities to identify performance issues and potential for further improvements.

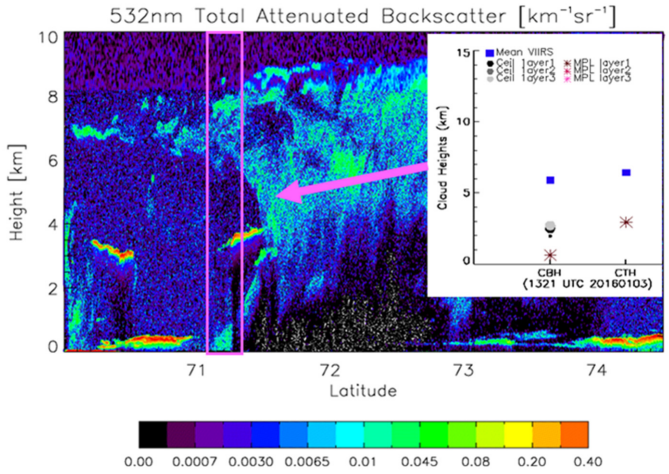

Figure 6. Comparison of S-NPP VIIRS CTH and CBH with CALIPSO lidar and ground ceilometer/lidar data for a multilayer cloud case near the ARM NSA site in Alaska as indicated in a pink rectangle (1321 UTC on 3 January 2016). Here, mean CTH and CBH from VIIRS (blue dots in the corner plot) only captured a topmost layer of the multilayered clouds, and ground ceilometer (black/gray circles) and lidar (brown/red asterisks) measurements reported lower-level layers.

Validation studies against spaceborne active sensor data and ground-based observations have revealed the need for further algorithm enhancements and more user-oriented product demonstration as highlighted in the following bullets.

- The performance of the current CBH/CCL retrieval is affected by the accuracy of the upstream cloud retrieval products used as algorithm input. The cloud algorithms, including CBH/CCL, operate on pixels determined to be 'cloudy' or 'probably cloudy' by the VIIRS Cloud Mask. False/missed clouds by the VIIRS cloud mask will be inherited by downstream cloud algorithms. CTH and CWP will directly impact the accuracy of CBH estimates and thus CCL products. Inaccurate upstream cloud retrievals will result in CBH failing to meet specifications.
- Nighttime performance is degraded relative to daytime, since NWP and IR-based data are used in lieu of visible band data, adding uncertainties in retaining the product consistency at night. This limitation has hindered the usage of these satellite data in the Arctic during the long and dark winter seasons despite high spatial and temporal coverage of the polar satellites at high latitudes. These issues can be mitigated in part via use of the VIIRS DNB on nights with available moonlight (Section 7).
- The current CBH algorithm has been optimized for single-layer clouds or the uppermost cloud layer by utilizing other upstream cloud properties. Multi-layered cloud systems present challenges to VIIRS cloud retrievals despite interests in user communities, particularly aviation, where lowest-cloud-layer detection can be critical. Therefore, the CBH and CCL products should be used with caution in regions where multi-layered clouds are present. Further research to improve the algorithm performance for multi-layered clouds is ongoing.
- Product validation for nighttime and multilayer cloud scenes is also challenging due to the lack of proper observational data. CloudSat provides cloud vertical observations, but a battery anomaly has resulted in daytime-only operation since 2011 [61]. CALIPSO lidar observations are limited in their ability to detect lower cloud levels below thick top layers and often experience anomalies (e.g., [62]). Surface-based measurements from ceilometers, radars, and lidars can provide intensive in situ data but are very limited in time and spatial coverage. Given various limitations in existing observation systems, more effective combinations of these data sets and investigation for new candidates should continue for validation and long-term monitoring.
- More user-friendly product demonstrations should be accommodated to maximize the use of these satellite products. Although the new products have been developed and improved utilizing innovative research approaches, the capabilities and applications are not fully demonstrated on the users' side. Outreach and improvements to provide relevant products and training/display tools meeting their needs should be explored through intensive user-developer interactions.

These topics continually motivate our evolving research priorities, as will be discussed in the following sections.

4. Improved Cloud Cover Layers with CBH

The CBH algorithm is used to improve CCL products by augmenting lower-layer cloud coverage below cloud top. The CCL, which describes fractional Low (L)-Middle (M)-High (H) layer information (defined by either pressure or height thresholds, depending on the user needs), was originally defined based on cloud top data only, and as such often missed lower parts of clouds. By using CGT retrieved from the statistical CBH algorithm, lower cloud layer fractions can be enhanced by introducing additional cloud coverage typically hidden below the cloud top. The products can classify layers by using a variety of prescribed thresholds based on pressure levels, or at flight levels for aviation community users with different units (hPa, km, or kilofeet).

Furthermore, with the availability of CBH information, the CCL product can be rendered at the native resolution of the cloud property retrievals instead of on a coarser grid (e.g., 3×3 pixels, to provide fractional L/M/H coverage using CTH information

alone). Examples of different thresholds used for each layer height range are shown in Figure 7. It is noted that two thresholds of 440 hPa (~6.5 km) and 680 hPa (~3–3.5 km) are used for the three-layer classification in the figure, following a definition of the International Satellite Cloud Climatology Project (ISCCP) [63].

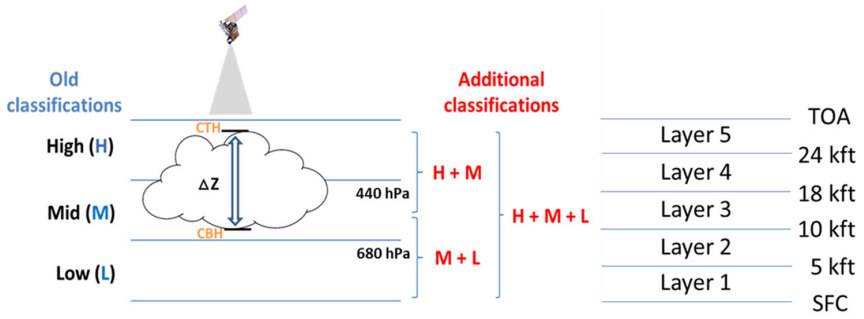

Figure 7. Expansion of cloud classifications from three to five flight-based level layers. In this example, the cloud shown on the left would previously be defined as a high cloud (H) in the original CCL product, but the introduction of CGT information in the new product allows it to be classified as high+mid (H+M), or as a cloud extending through flight layers 3, 4 and 5.

The improved CCL Product applies to various sensors including VIIRS and GOES-R ABI, and provides new information about the deep parts of a cloud, such as convective cloud layers that can produce both in-cloud and clear-air turbulence hazards of interest to the aviation community. Figure 8 shows samples of cloud layer fractions (0–1 range) from S-NPP VIIRS over Alaska at 1355 UTC on 29 June 2016 for each layer L/M/H cloud layer bin when only CTH is used to calculate the fractions and when the CBH information is included, respectively. The figure shows increased middle and low layer cloud fractions, particularly over deep convective areas by including the new CBH. These results confirm how the new CBH augments lower-level cloud fractions hidden under the cloud top. Additional cloud layers are indicated by mnemonic designators indicating vertical cloud extent; for example, "H+M+L" means that high, mid, and low cloud is present in the field of view of the pixel, and so on (Figure 9). The previous CCL Product only allowed one of the high, mid, or low cloud categories to be designated, leaving out important data on the vertical extent that can impact flight planning and safety.

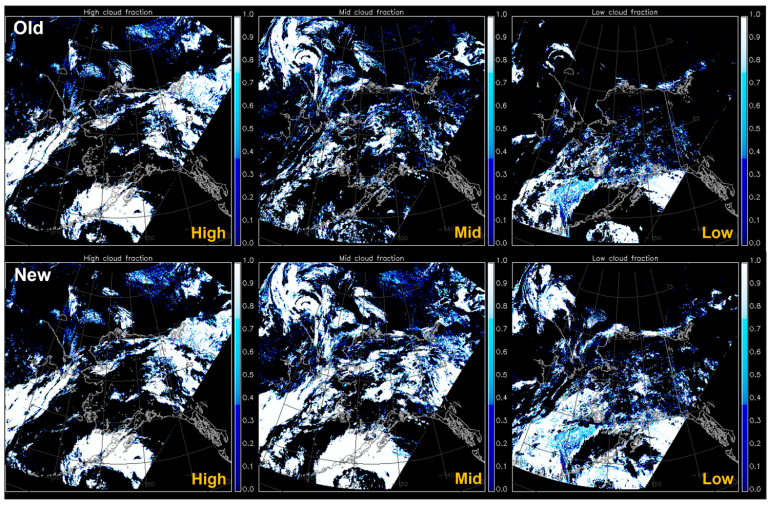

Figure 8. Comparison of cloud fractions from S-NPP VIIRS over Alaska (1355 UTC 29 June 2016) with and without cloud base information, respectively. The top panels show cloud fractions (0–1) only from cloud top heights for each low, middle, and high layer, and the bottom panels show increased middle and low layer cloud fractions by using the new CBH information.

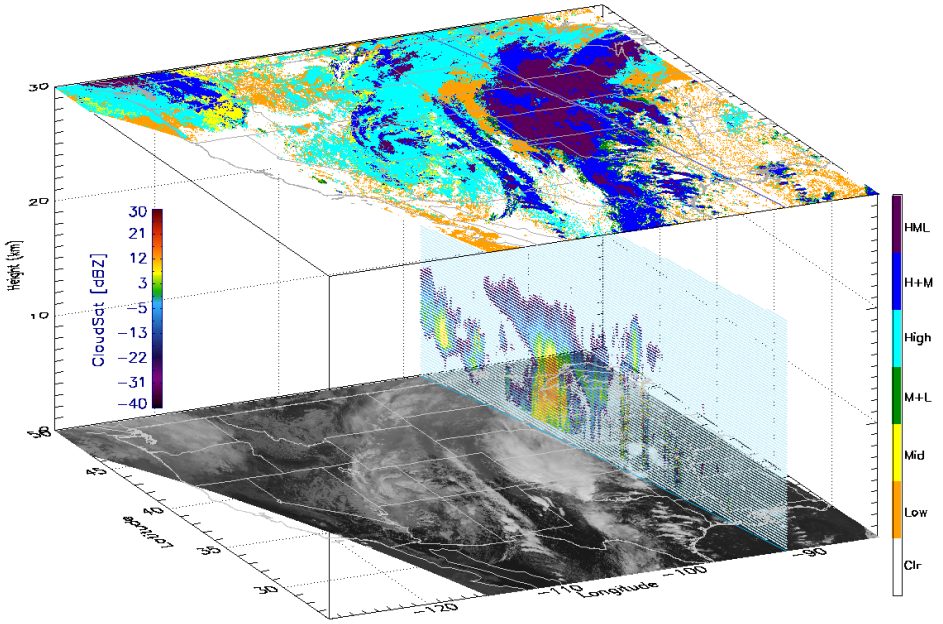

Figure 9. Sample of the improved NOAA Enterprise Cloud Cover Layers (CCL) Product from S-NPP VIIRS over the central U.S. (1954 UTC on 7 October 2018) together with a CloudSat overpass cross-section showing the detailed cloud top, cloud base, and vertical layer information. The newly enhanced CCL includes vertically extended layer categories such as High+Low, High+Mid, Mid+Low, and High+Mid+Low.

5. Further Refinements of CCL Using Machine Learning

Our CBH and CCL techniques are applicable to geostationary satellite sensors such as the GOES-16, -17, and -18 ABIs. However, it remains challenging to determine the CTH of the uppermost cloud layer in some multi-layered cloud systems, and it is difficult to identify, let alone quantify, the height of underlying cloud layers from passive satellite observations.

Since multi-layered cloud systems occupy a large portion of the globe (e.g., [64]) and are of particular relevance to the aviation community, they cannot be neglected. To begin addressing these challenging cloud scenarios, we have developed a machine learning (ML) based algorithm to detect the presence of a low-level cloud in the atmospheric column, which takes into account multispectral information from the ABI as well as vertical profiles of NWP relative humidity (RH) data. Details of the algorithm can be found in Haynes et al. [57], and are summarized briefly here.

This algorithm, like the statistical algorithm previously described, is based on matchups between passive sensors (in this case the ABI) and the radar and lidar-derived cloud boundaries from CloudSat and CALIPSO. The approach applies Random Forest (RF) and Artificial Neural Networks (ANN) to GOES ABI data and NWP model relative humidity (RH) data that are trained with the aforementioned CloudSat and CALIPSO cloud boundaries as "truth." RH is included as a predictor because it is correlated with cloud occurrence. We want to avoid hardcoding RH thresholds into the algorithm, though, as these thresholds vary regionally and by season. Rather, we provide them as inputs to the ML algorithm, with the hope that the model will learn to use this information in an optimal fashion.

As demonstrated by Haynes et al. [57], the RF and ANN neural networks perform similarly, so the RF was chosen for operational implementation given the relative simplicity of this framework. When applied to an independent testing dataset, the probability of detection (PoD) of low clouds increased from 0.185 to 0.685 relative to the statistical CCL algorithm that was previously described, while the false alarm ratio (FAR) decreased. For those scenes that the ABI identified as "cirrus" (one of the most difficult scenarios for multilayer detection), the PoD increase was slightly more pronounced (0.183 to 0.686).

Beyond Haynes et al. [57], some changes have been made to make the algorithm faster, allow operation at night, and ease transition of the algorithm to VIIRS. The daytime algorithm uses the following predictors:

- ABI channels 1–6, 13 (0.47, 0.64, 0.87, 1.38, 1.61, 2.25, 10.35 μm)
- NWP profiles of relative humidity (maximum between 1000 and 600 hPa, and at 150 hPa)
- Solar zenith angle and latitude

The nighttime algorithm differs in that only infrared channels are used. In the full version of the algorithm, a slight performance degradation at night was demonstrated [57].

It is noteworthy (and by design) that each of these ABI channels has a corresponding VIIRS channel in the same spectral range. The team is working on translating this method, initially developed in association with the GOES-R Proving Ground, to use VIIRS channels as inputs. A preliminary application of the ABI model to VIIRS data, and the corresponding change in the CCL product, is shown in Figure 10. In this example, the trained daytime ABI model was applied to the nearest VIIRS M-band channel (although for greater accuracy it will be necessary to account for calibration differences and differing spectral response functions between the two instruments). Low cloud detections from the ML algorithm were used to supplement the predictions based on the non-ML, statistical cloud base algorithm. Two main differences are evident when ML is included: significant areas of H+M are transitioned to H+M+L as ML-detected low clouds are added, and areas of H+L clouds are newly produced. The results show that the ML algorithm can contribute to identifying low cloud presence which has important aviation and various meteorological implications.

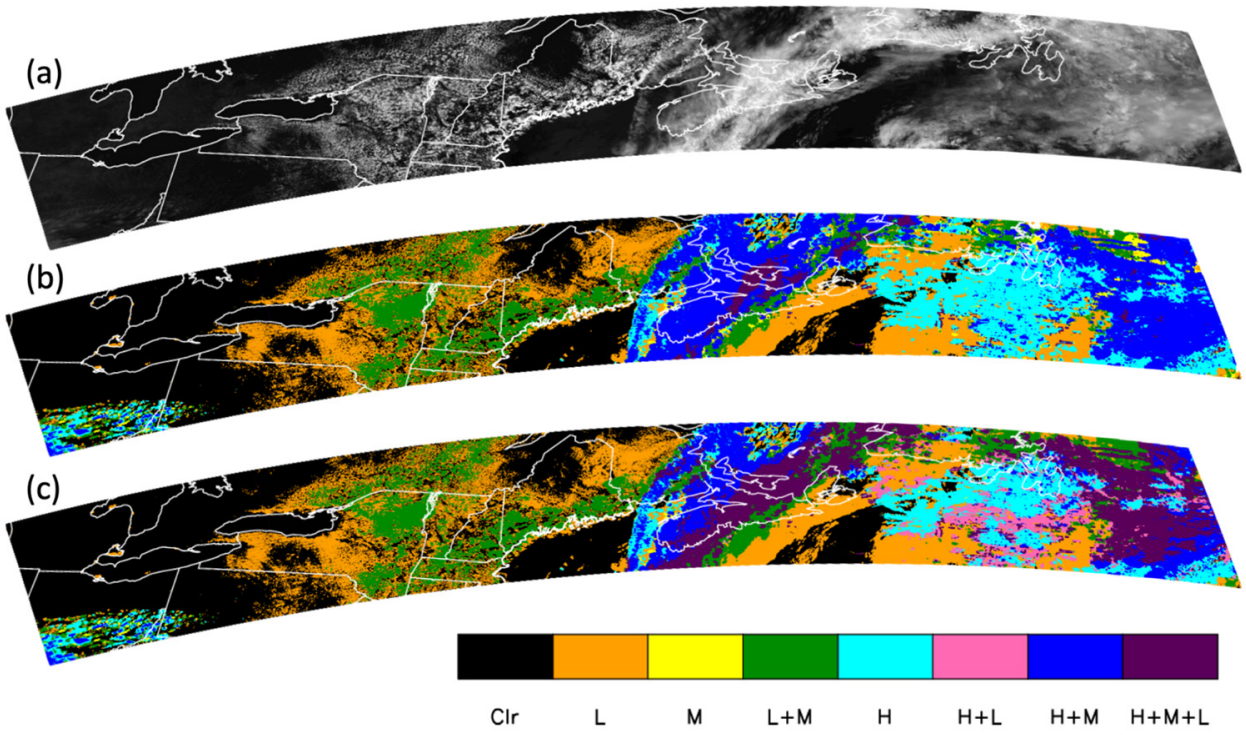

Figure 10. Example CCL product for NOAA-20 VIIRS at 1718 UTC on 28 June 2022. (**a**) Channel M5 (0.672 μm) reflectance, (**b**) CCL product without machine learning model, and (**c**) CCL product with machine learning model applied. Colorbar refers to cloud layer categories in (**b**,**c**).

6. User Engagement for the Aviation Applications

The improved CBH and CCL products can provide more information about what occurs in vertically extended cloud layers that pilots might encounter at their flight level. Pilots must follow a specific set of rules, established by the Federal Aviation Administration

(FAA) in the United States and other agencies internationally, to operate aircraft in different weather conditions. Visual Flight Rules (VFR) restrict pilots from flying through clouds because they must maintain horizontal visibility of three to five miles (~5–8 km). VFR requires that they must either fly under, over, or divert around clouds if they intercept their route ("see and avoid"). In contrast, Instrument Flight Rules (IFR) allow pilots to use cockpit instruments to navigate a plane through clouds and rough weather conditions. CCL information enables pilots to anticipate areas of clouds that could turn a VFR flight into an IFR one, which is important for flight planning and in-flight adjustments. Understanding cloud layer conditions also helps pilots anticipate problems with terrain that are hidden in the clouds and may not be visible to the pilot, particularly for VFR and in the rare scenario of an on-board instrument failure.

Leveraging the early success of the advanced CBH and CCL products, we have continued further improvements to provide optimized retrievals for users. Through ongoing efforts, we recently introduced VIIRS Cloud Vertical Cross-section (CVC) products along flight paths for the Alaska region, supporting the NOAA JPSS Aviation Initiative which encourages user-developer interactions for effective product transition to operations. Recognizing the need for improved forecasting of aviation hazards, NOAA established the JPSS Aviation Initiative in 2018 with a focus on engaging pilots and aviation forecasters in Alaska. This initiative helps the polar aviation community by providing new and improved satellite products, while also facilitating collaborations with end users.

In support of this initiative, we have been working on new approaches to enhance satellite cloud information. This is an experimental product demonstration to provide vertically extended cloud structure information that forecasters can easily access, interrogate, and interpret for aviation applications. Focusing on the needs of aviation users in the data-sparse region at high latitudes (and looking toward the future extension to CONUS and global scales), we aim to provide aviation-focused satellite observations beyond typical 2D plan-view imagery.

NOAA offers a great number of satellite cloud products in their Enterprise Cloud Product Package, and other operational agencies provide a similar variety of data sets. With the numerous meteorological data resources given to forecasters and aviation users, "data overload" can occur, so it is necessary to deliver data in a user-friendly format. Our experimental CVC product is a preliminary attempt to provide a comprehensive 3D cloud data set for aviation applications. With an S-NPP or NOAA-20 satellite overpass of Alaska, cross-sections of cloud information along selected flight paths from VIIRS are linked to a website (https://rammb.cira.colostate.edu/ramsdis/online/npp_viirs_arctic_aviation.asp (accessed on 1 November 2022)).

The website graphically displays a vertical view of cloud properties along popular aviation routes, including cloud boundaries, cloud conditions, and terrain. Turbulence and icing conditions from pilot reports (PIREPs) and NOAA Unique Combined Atmospheric Processing System (NUCAPS; [65–67]) temperature data are added to the cross-sections when available. If the NUCAPS temperature data are not available or invalid, NWP model data are used. As shown in Figure 11, the product is regularly adjusted and improved based on user feedback, and the cloud cross-sections help pilots understand how far clouds might extend toward the surface and thus better understand hazardous conditions in their path. Provided below is a quote from a NASA online news article [68] on this research effort including an interview message below from Adam White—an Alaska pilot, a government liaison for the Alaska Airmen's Association, and a participant in the JPSS Aviation initiative:

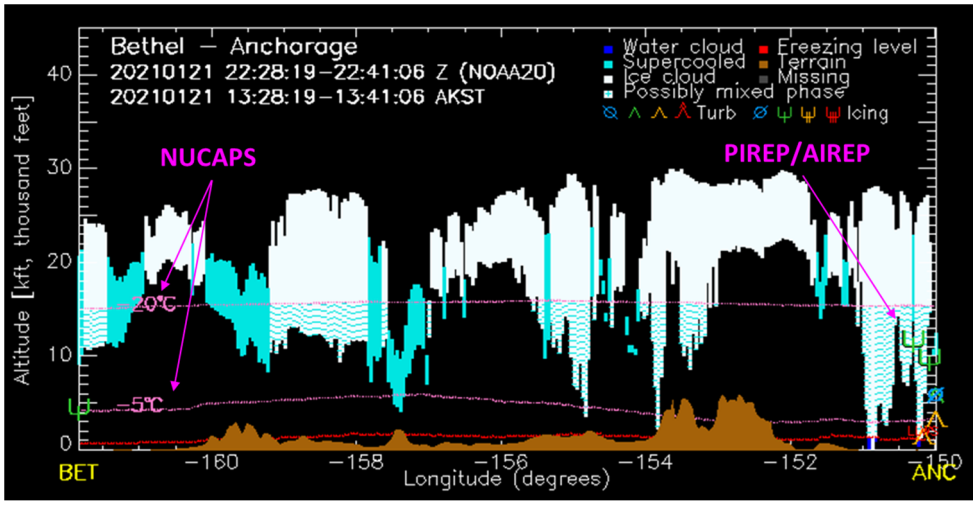

Figure 11. Sample cloud vertical cross-section between Bethel and Anchorage, Alaska from NOAA-20 VIIRS at 2228 UTC on 21 January 2021.

> *"While the tops of clouds are important, I need to know what the clouds are made of, and I need to know how far down they go and how close they are to the ground, and this is the first time we've had a product that helps us answer these questions. I've made decisions not to fly on a particular day because of what this product has shown me, even in the testing phase. It's saved me from potential problems, whether it's icing or clouds down to the ground that I wouldn't be able to navigate." (Adam White, Alaska Airmen's Association)*

Initially, the Cloud Vertical Cross-section product was only available along popular flight routes in Alaska. It has since been extended to more pre-selected paths over the lower 48 states in the U.S.; for example, Seattle to Denver (https://rammb.cira.colostate.edu/ramsdis/online/npp_viirs_conus_aviation.asp (accessed on 1 November 2022)).

Recognizing the value of this information, aviation users requested the option to select custom routes. In response to the user request, we launched a fully interactive website (https://aviation.cira.colostate.edu/) that allows users to select two or more latitude/longitude way-points on a map and create a cloud vertical cross-section for that route as shown in Figure 12. The website includes a "user quick guide" that has been updated with feedback from Alaska local pilots, and a user-feedback option to provide researchers with direct feedback on any cross-section that is generated.

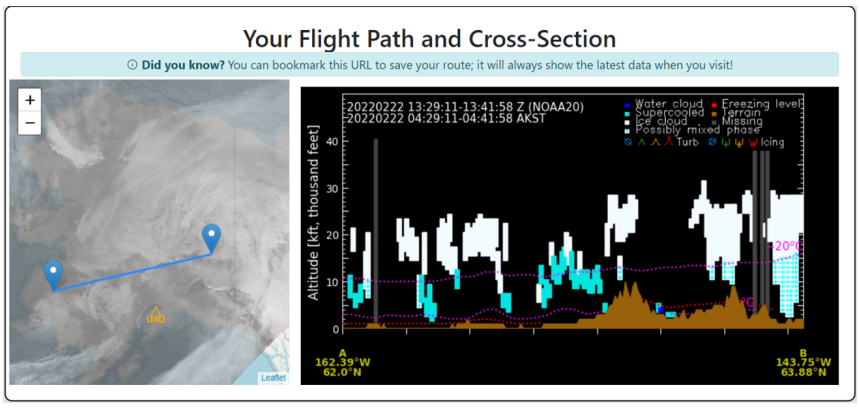

Figure 12. Sample Cloud Vertical Cross-section product from the CIRA new aviation website that allows users to select routes of their choice on a map to create a custom cross-section displaying cloud phase, altitude, terrain, turbulence, and icing information (https://aviation.cira.colostate.edu/, accessed on 31 October 2022).

Allowing users to generate their customizable cloud cross-sections required additional data processing, including the back-end construction of a fully gridded, 3D cloud dataset. A preliminary interpolation process was developed to generate one gridded 3D cloud field from the various datasets used for CVCs. Figure 13 shows a schematic diagram of the 3D cloud data processing. We are currently using a horizontal resolution of $0.02^\circ \times 0.02^\circ$ with 51 vertical levels at 1000 ft resolution. Typical nearest neighbor and inverse-distance weighting interpolations are used, and the output is saved with compact 16-bit integers into a NetCDF file. CVCs are updated every time there is a JPSS satellite overpass, so users can watch for changing conditions. Archived cross-sections dating back four weeks are available for pre-selected routes. The custom cross-section product is currently available for Alaska, and preliminary output is also shown for other U.S. regions.

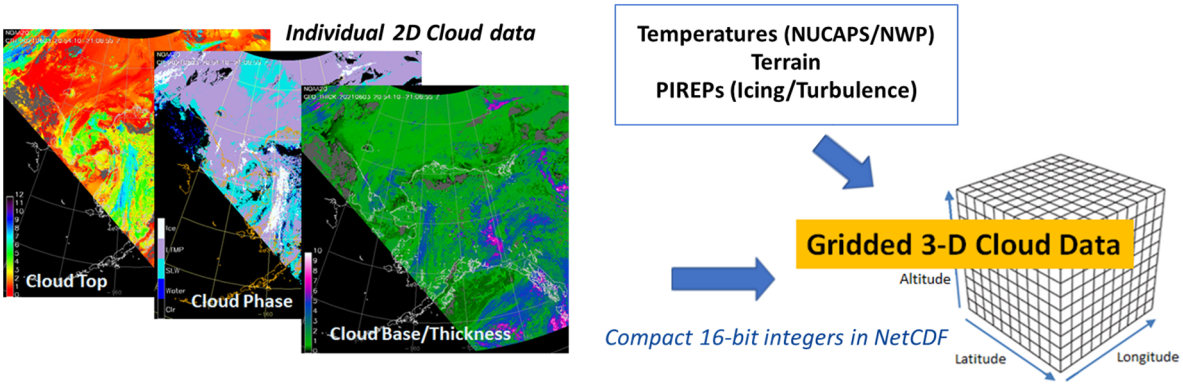

Figure 13. Schematics of the new 3-D gridded cloud data field generated from multiple cloud products, temperatures, and terrain data together with PIREPs (icing and turbulence).

User feedback based on the real-life experiences of aviation users is essential for making further meaningful improvements to the new products. The products receive regular feedback from Alaska users and have been improved through active user interactions, reflecting the initial goal of increasing the utility of the JPSS cloud products to aviation users. Forecasters can also benefit from the enhanced capabilities. We strive to engage users of our aviation weather products, ranging from pilots and aviation meteorologists, through direct communication, social media, and online surveys.

Working with end users has been necessary to improve and evaluate new satellite products and to transition products from research to societal benefit. One report from an Alaska pilot used in product evaluation, which revealed a high bias of the CBH estimator for this case, is shown below.

> *"I took off from FAI (Fairbanks International Airport) at 2300Z Sept 21 and landed at MRI (Merrill Field Anchorage) at 0100Z Sept 22 (3 pm to 5 pm AKDT). I observed no ceiling from FAI to the Alaska Range foothills, which is basically in agreement with the cross-sections. By the time I was over Totatlanika River strip (9AK) I was under scattered to broken clouds with bases around 5500 ft MSL. Basically, I flew under a broken to overcast ceiling that was at about 5500 to 6000 ft nearly all the way from McKinley Park (PAIN) to about Willow (PAOU). These bases were considerably lower than shown on the cross-sections for most of the route..." (an email report from an Alaskan pilot)*

The products have been used as supplementary observational data to investigate aviation accidents. For example, an accident occurred around 2251 UTC on 16 August 2021 near Fairbanks, Alaska. A small plane carrying eight passengers and a pilot encountered severe turbulence that caused flight control issues. The pilot landed safely with no reported injuries, but the aircraft's wing was significantly damaged. During its investigation, the National Transportation Safety Board (NTSB) used archived Cloud Vertical Cross-sections and NOAA-20 VIIRS Infrared imagery to assess flight path conditions along the route and

found that wing ice contributed to the accident. Icing conditions along the route are shown in cyan (supercooled liquid cloud) on the archived cross-sections in Figure 14.

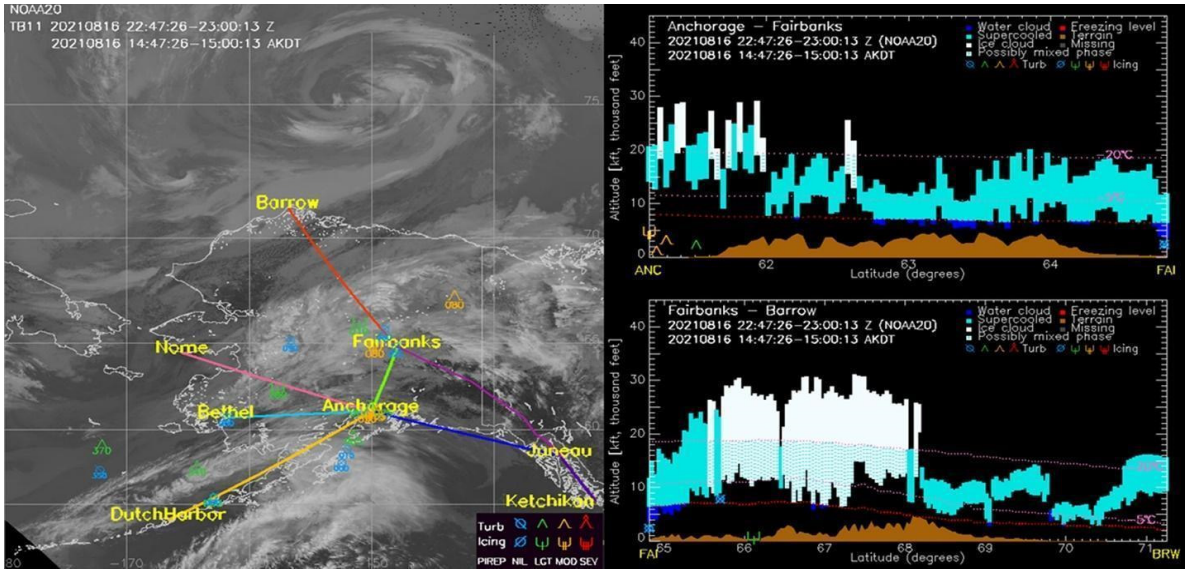

Figure 14. NOAA-20 VIIRS Infrared imagery (**left**) and cloud cross-sections along two flight paths between Anchorage and Fairbanks, and Fairbanks and Utqiagvik-Barrow, Alaska (**right**) used in the NTSB accident investigation which occurred around 2251 UTC on 16 August 2021 near Fairbanks.

7. Improvement of Nighttime Performance with DNB Data

Nighttime algorithm performance suffers from a lack of reliable CWP data. Conventional retrieval approaches for daytime cloud optical properties used to compute CWP have been well developed [69–71] but still show limited performance at night [72].

Refinements for nighttime CBH/CCL retrievals using VIIRS Day/Night Band (DNB) [73] have been explored as a continuing effort to provide improved nighttime retrievals, concentrating on the needs of operational users and pilots in high latitude data-sparse regions such as Alaska during dark winter months, with the high temporal resolution provided by JPSS satellites filling a data gap where data coverage from geostationary satellites is limited.

In the statistical CBH algorithm, CBH is generated by subtracting CGT from CTH. Here, CGT is retrieved from the lookup table utilizing CWP as input. Together with CTH, consistent CWP information (from cloud optical properties, COT and EPS) is important to derive accurate CGT and thus CBH in the algorithm. Since IR brightness temperatures quickly saturate in cloudy scenes, these measurements provide little information about the CWP. In contrast, the weak absorption of both liquid and ice-phase clouds provides a tractable way to derive CWP via reflected sunlight during the day. The problem is far more challenging at night due to the lack of visible light.

We have been utilizing capabilities of the NLCOMP retrievals [71,72] with VIIRS DNB based on a lunar reflectance model by Miller and Turner [73,74], which are embedded in the CLAVR-x system. The VIIRS DNB has provided a unique opportunity to overcome many limitations in nighttime cloud observations [74,75]. With enhanced CWP input from the NLCOMP algorithm with DNB, we have improved the quality of nighttime CBH/CCL retrievals during periods with sufficient lunar illumination. These products generated from CLAVR-x are available at CIRA's Polar SLIDER and VIIRS websites. When moonlight is not sufficient, an NWP-based CWP estimate is provided as input for the CBH algorithm. When NWP data do not provide a cloud properly at the cloudy pixel location (often for very thin cloud cases), the extinction-based CBH [50] can be used alternatively. Sample CGT retrievals using CWPs from NLCOMP with DNB and NWP data are shown in Figure 15. This updated algorithm enlisting DNB lunar information in place of purely NWP-based

CWP at night will be included in the operational release through the NOAA CLASS (VIIRS operational cloud product version-v3r2).

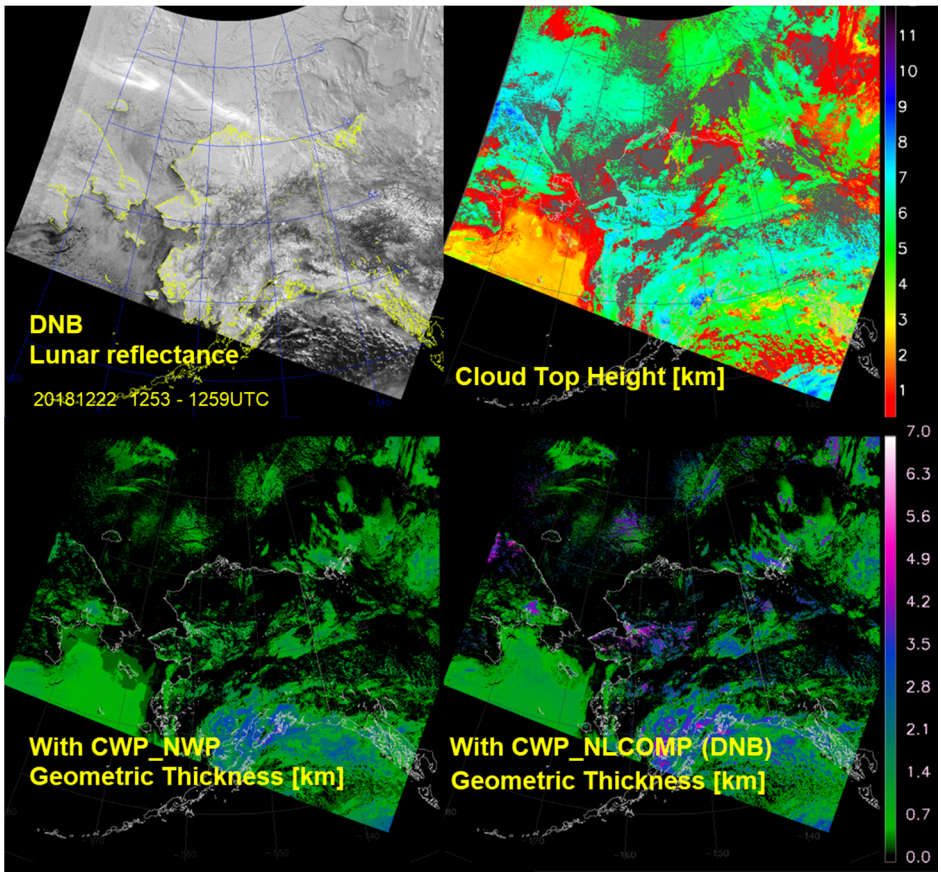

Figure 15. Comparison of CGT values showing deeper cloud thickness can be retrieved by using VIIRS Day/Night Band data (**bottom right**) over conventional CGT nighttime retrieval with NWP-based CWP input (**bottom left**) over Alaska. The top panels show VIIRS DNB lunar reflectance and CTH from S-NPP at 1253 UTC on 22 December 2018.

8. Future Work

As this vertical cloud distribution is more fully developed, opportunities for new products will become possible. For example, we aim to quantify not only the vertical location of clouds, but also the water content of these clouds. The ability to retrieve vertical distributions of water content from a passive sensor would be particularly useful for detecting dangerous aircraft icing conditions. To this end, we are currently exploring the use of ANNs and convolutional neural networks (CNNs; [76]), including U-Net architectures [77], to derive the vertical distribution of cloud liquid and ice within the VIIRS footprint, as constrained by the cloud water path derived for the scene. The training for these datasets is the cloud water content retrievals from the radar onboard CloudSat, matched to VIIRS observations.

On moonless nights, the current CBH accuracy becomes highly dependent on the corresponding NWP data accuracy. As part of ongoing research for improved nighttime retrievals, we are exploring the use of the Advanced Technology Microwave Sounder (ATMS) data as an alternative to NWP data. This multi-sensor/model-fusion approach has been utilized to overcome traditional IR-based retrieval limitations at night. The ATMS CWP data from S-NPP and NOAA-20 is processed at a higher resolution of ~15 km (at nadir) through the NOAA operational Microwave Integrated Retrieval System (MiRS) [78,79]. It is noted that the operational ATMS water path data are valid for non-precipitating clouds only, and its performance over land is limited. Statistical regression analyses of CWP parameters

from VIIRS DNB (NLCOMP) and ATMS together with NWP (currently the NOAA Global Forecast System (GFS) model) and IR CWP data are ongoing for full moon periods over Alaska. Ocean-only data are currently used to avoid errors associated with land and sea ice reflectance and emission contributions. Further new approaches including a machine learning approach (such as RF [80]) are being tested in parallel to effectively combine these multiple data sets which have non-linear characteristics with different resolutions. The fusion of these data will be explored for potential updates.

Through validation against other satellites and ground-based measurements, detailed uncertainty and error analysis has been performed for the long-term stability of the algorithm and products. In future validation studies, additional space-borne active sensor data will be utilized to analyze the 3-D cloud structure over larger domains, as allowed by data availability. Data sources we will use include the Earth Cloud Aerosol and Radiation Explorer mission (EarthCARE [81]; launch scheduled for 2023) by the European Space Agency (ESA) and the Japan Aerospace Exploration Agency (JAXA), carrying lidar and radar. The Dual-frequency Precipitation Radar (DPR) onboard the Global Precipitation Measurement (GPM) mission [82] could be utilized for the southern Alaska region (up to ~65°N) and CONUS for limited case studies, taking into account its relative insensitivity to clouds compared to precipitation.

9. Summary

Conventional passive radiometers offer a ready means to assess cloud-top properties but have traditionally been limited in their capability to provide the 3D cloud structure information required by various aviation weather applications as well as climate studies. Tied with JPSS VIIRS research over the last ten years, we have developed a statistical, semi-empirical CBH algorithm based on a global analysis of active and passive sensor-combined satellite observations. The new algorithm has been demonstrated to outperform the initial IDPS CBH algorithm through intensive validation studies. The new CBH algorithm is currently operational as part of the NOAA Enterprise Cloud Algorithms. The algorithm development and validation efforts were overviewed in this paper.

With the successful implementation of the CBH algorithm into NOAA JPSS operations, VIIRS cloud products have been demonstrated to Alaska aviation users as part of the NOAA JPSS Aviation Initiative efforts, which included the Enterprise CBH and improved CCL. The aviation community has relied on pilot reports about observational cloud conditions hidden under the cloud top in the atmosphere. Understanding the cloud properties from top to bottom is essential for pilots to avoid hazardous weather situations, and the lack of vertical data is a key consideration in preparing their flight plans in case of severe weather conditions. An initial goal of our work was to maximize the benefits and performance of JPSS cloud products, particularly in terms of providing more comprehensive 3D cloud structure information with CBH/CCL products and taking advantage of increased temporal coverage from JPSS satellites, S-NPP, NOAA-20, and the upcoming JPSS-2 (slated for launch in late 2022).

By directly interacting with aviation users, we obtained valuable feedback and insights that allowed us to optimize a new approach to provide satellite-based 3D cloud data. Due to the coarse aviation observational network in this region and, as often affirmed by comments from NOAA operational forecasters and aviation users, satellite-derived cloud products are extremely helpful in filling significant observational gaps. Focusing on user needs, the work could step forward to provide more practical satellite cloud products in a user-friendly, user-driven format in this data-sparse region.

The experimental CVC product adds a vertical dimension to the traditional 2D cloud retrieval products, which is the first to offer pilots the ability to see what is happening inside a cloud along a flight path based on satellite observations. The products are obtained by combining multiple Enterprise cloud products from VIIRS together with supplementary data beneficial for aviation users, such as temperatures related to icing as well as PIREPs,

with an eye toward providing a comprehensive, expandable data package based on satellite cloud observations.

These products not only benefit the aviation community, but are also useful for weather and climate modeling. Frequent feedback and interactions from aviation users have enabled further refinements of the products and training/display tools for users. Building on this feedback and collaboration, additional features and improvements to the CVC product and user interfaces have been pursued, including user-selectable cloud cross-section features based on 3D gridded satellite cloud data and extending this effort to global coverage. Feedback also drives future efforts and products. We continue to hone additional approaches for the current CBH and CCL algorithms including the use of machine learning for improved multi-layer cloud retrievals and refinement of nighttime performance.

This work represents an initial step to creating a new generation of satellite-based cloud products for the whole weather and climate research community as well as aviation users. The ultimate goal is to provide users with additional, high-quality vertical cloud information in the atmosphere. Improved weather monitoring and forecast capabilities at high latitudes including Alaska, where we started this satellite-based 3D cloud research, are vitally important for commerce and transportation growth and to protect the safety of both residents and workers in this region marked by weather extremes and a changing climate. JPSS satellite cloud products provide a wealth of quantitative observations necessary for improving our fundamental understanding of cloud vertical structures, and are helping improve aviation weather applications in data-sparse regions. This work will contribute to improving our scientific understanding of global clouds and provide practical use of satellite-based cloud products. While this work was initiated in Alaska, we expect it will benefit the entire globe when fully deployed. Due in large part to the contributions and feedback from a highly engaged user community, the future is bright for the continued development of JPSS-supported satellite-based innovations for the meteorological and aviation communities.

Author Contributions: Conceptualization, investigation, validation, writing—original draft preparation, Y.-J.N.; investigation, methodology, writing—review and editing, J.M.H. and C.J.S.; methodology, supervision, writing—review and editing, S.D.M.; conceptualization, resources, funding acquisition, A.K.H.; resources, administration, J.W.; writing—review and editing, funding acquisition, M.S.K.; software, visualization, M.N. and B.J.D. All authors have read and agreed to the published version of the manuscript.

Funding: This work has been supported by the JPSS Program Office through the NOAA/NESDIS/Center for Satellite Applications and Research under NOAA Award (NA19OAR4320073).

Data Availability Statement: S-NPP and NOAA20 VIIRS CBH and CCL data are publicly available at the NOAA Comprehensive Large Array-data Stewardship System (CLASS; https://www.class.noaa.gov (accessed on 31 October 2022)), which can be found under "JPSS VIIRS Sensor Data Record Operational (VIIRS_SDR)". The VIIRS imagery and cloud products used in this study are also available in CIRA's SLIDER (https://rammb-slider.cira.colostate.edu (accessed on 31 October 2022)) and the Experimental Aviation website (https://aviation.cira.colostate.edu (accessed on 31 October 2022)).

Acknowledgments: The authors would like to thank collaborators and Alaska aviation users: William Straka, Yue Li, Steve Wanzong (all from Cooperative Institute for Meteorological Satellite Studies; CIMSS), Tom George (Aircraft Owners and Pilots Association), Adam White (Alaska Airmen's Association), Becca Mazur (NOAA Arctic Testbed), Carl Dierking, Jay Cable, Jen Delamere (all from Cooperative Institute for Climate, Ocean, and Ecosystem Studies; CICOES, formerly University of Alaska Fairbanks/Geographic Information Network of Alaska; GINA), Amanda Terborg, Ty Higginbotham (both from NOAA Aviation Weather Center/Aviation Weather Testbed), Nadia Smith, Rebekah Esmaili, Amy Leibrand (all from Science and Technology Corporation /NOAA), Jenny Colavito (Federal Aviation Administration), Paul Suffern (National Transportation Safety Board; NTSB), and Jeremy Goldstein (Global Science and Technology, Inc.).

Conflicts of Interest: The views, opinions, and findings contained in this report are those of the authors and should not be construed as an official NOAA or U.S. Government position, policy, or decision.

References

1. Smith, W.L.; Minnis, P.; Fleeger, C.; Spangenberg, D.; Palikonda, R.; Nguyen, L. Determining the flight icing threat to aircraft with single-layer cloud parameters derived from operational satellite data. *J. Appl. Meteorol. Climatol.* **2012**, *51*, 1794–1810. [CrossRef]
2. Smith, T.M.; Lakshmanan, V.; Stumpf, G.J.; Ortega, K.L.; Hondl, K.; Cooper, K.; Calhoun, K.M.; Kingfield, D.M.; Manross, K.L.; Toomey, R.; et al. Multi-Radar Multi-Sensor (MRMS) Severe Weather and Aviation Products: Initial Operating Capabilities. *Bull. Am. Meteorol. Soc.* **2016**, *97*, 1617–1630. [CrossRef]
3. Randall, D.A. Cloud parameterization for climate models: Status and prospects. *Atmos. Res.* **1989**, *23*, 345–362. [CrossRef]
4. Heidinger, A.K.; Pavolonis, M.J. Gazing at cirrus clouds for 25 years through a split-window. Part I: Methodology. *J. Appl. Meteorol. Climatol.* **2009**, *48*, 1100–1116. [CrossRef]
5. Noh, Y.J.; Miller, S.D.; Heidinger, A.K.; Mace, G.G.; Protat, A.; Alexander, S.P. Satellite-based detection of daytime supercooled liquid-topped mixed-phase clouds over the Southern Ocean using the Advanced Himawari Imager. *J. Geophys. Res.* **2019**, *124*, 2677–2701. [CrossRef]
6. Zelinka, M.D.; Myers, T.A.; McCoy, D.T.; Po-Chedley, S.; Caldwell, P.M.; Ceppi, P.; Klein, S.A.; Taylor, K.E. Causes of Higher Climate Sensitivity in CMIP6 Models. *Geophys. Res. Lett.* **2020**, *47*, e2019GL085782. [CrossRef]
7. Forsythe, J.M.; Vonder Haar, T.H.; Reinke, D.L. Cloud-base height estimates using a combination of meteorological satellite imagery and surface reports. *J. Appl. Meteorol.* **2000**, *39*, 2336–2347. [CrossRef]
8. Marzban, C.; Leyton, S.; Colman, B. Ceiling and visibility forecasts via neural networks. *Weather Forecast.* **2007**, *22*, 466–479. [CrossRef]
9. Heidinger, A.K.; Foster, M.J.; Walther, A.; Zhao, X.T. The Pathfinder Atmospheres–Extended AVHRR Climate Dataset. *Bull. Am. Meteorol. Soc.* **2014**, *95*, 909–922. [CrossRef]
10. Kalluri, S.; Cao, C.; Heidinger, A.; Ignatov, A.; Key, J.; Smith, T. The Advanced Very High Resolution Radiometer: Contributing to Earth Observations for over 40 Years. *Bull. Am. Meteorol. Soc.* **2021**, *102*, E351–E366. [CrossRef]
11. King, M.D.; Tsay, S.-C.; Platnick, S.E.; Wang, M.; Liou, K.N. Cloud Retrieval Algorithms for MODIS: Optical Thickness, Effective Particle Radius, and Thermodynamic Phase. MODIS Algorithm Theoretical Basis Document, ATBD-MOD05. December 1997. Available online: https://eospso.nasa.gov/sites/default/files/atbd/atbd_mod05.pdf (accessed on 25 August 2022).
12. Menzel, W.P.; Frey, R.A.; Zhang, H.; Wylie, D.P.; Moeller, C.C.; Holz, R.E.; Maddux, B.; Baum, B.A.; Strabala, K.I.; Gumley, L.E. MODIS Global Cloud-Top Pressure and Amount Estimation: Algorithm Description and Results. *J. Appl. Meteorol. Climatol.* **2008**, *47*, 1175–1198. [CrossRef]
13. Bessho, K.; Date, K.; Hayashi, M.; Ikeda, A.; Imai, T.; Inoue, H.; Kumagai, Y.; Miyakawa, T.; Murata, H.; Ohno, T.; et al. An introduction to Himawari-8/9—Japan's new-generation geostationary meteorological satellites. *J. Meteorol. Soc. Jpn.* **2016**, *94*, 151–183. [CrossRef]
14. Schmit, T.J.; Griffith, P.; Gunshor, M.M.; Daniels, J.M.; Goodman, S.J.; Lebair, W.J. A closer look at the ABI on the GOES-R series. *Bull. Am. Meteorol. Soc.* **2017**, *98*, 681–698. [CrossRef]
15. Yang, J.; Zhang, Z.; Wei, C.; Lu, F.; Guo, Q. Introducing the new generation of Chinese geostationary weather satellites–FengYun 4 (FY-4). *Bull. Am. Meteorol. Soc.* **2017**, *98*, 1637–1658. [CrossRef]
16. Kim, D.; Gu, M.; Oh, T.-H.; Kim, E.-K.; Yang, H.-J. Introduction of the Advanced Meteorological Imager of Geo-Kompsat-2a: In-Orbit Tests and Performance Validation. *Remote Sens.* **2021**, *13*, 1303. [CrossRef]
17. McCleese, D.J.; Wilson, L.W. Cloud top height from temperature sounding instruments. *Q. J. R. Meteorol. Soc.* **1976**, *102*, 781–790. [CrossRef]
18. King, M.D.; Menzel, W.P.; Kaufman, Y.J.; Tanre, D.; Gao, B.C.; Platnick, S.; Ackerman, S.A.; Remer, L.A.; Pincus, R.; Hubanks, P.A. Cloud and aerosol properties, precipitable water and profiles of temperature and water vapor from MODIS. *IEEE Trans. Geosci. Remote Sens.* **2003**, *41*, 442–458. [CrossRef]
19. Baum, B.; Menzel, W.P.; Frey, R.; Tobin, D.; Holz, R.; Ackerman, S. MODIS Cloud Top Property Refinements for Collection 6. *J. Appl. Meteorol. Climatol.* **2012**, *51*, 1145–1163. [CrossRef]
20. Vislocky, R.L.; Fritsch, J.M. An automated, observations-based system for short-term prediction of ceiling and visibility. *Weather Forecast.* **1997**, *12*, 31–43. [CrossRef]
21. Hansen, B. A fuzzy logic–based analog forecasting system for ceiling and visibility. *Weather Forecast.* **2007**, *22*, 1319–1330. [CrossRef]
22. Miller, S.D.; Forsythe, J.M.; Partain, P.T.; Haynes, J.M.; Bankert, R.L.; Sengupta, M.; Mitrescu, C.; Hawkins, J.D.; Vonder Haar, T.H. Estimating three-dimensional cloud structure via statistically blended satellite observations. *J. Appl. Meteorol. Climatol.* **2014**, *53*, 437–455. [CrossRef]
23. Inoue, M.; Fraser, A.D.; Adams, N.; Carpenter, S.; Phillips, H.E. An assessment of numerical weather prediction–derived low-cloud-base height forecasts. *Weather Forecast.* **2015**, *30*, 486–497. [CrossRef]
24. Ellrod, G.P. Estimation of low cloud base heights at night from satellite infrared and surface temperature data. *Natl. Weather Dig.* **2002**, *26*, 39–44.

25. Mecikalski, J.R.; Feltz, W.F.; Murray, J.J.; Johnson, D.B.; Bedka, K.M.; Bedka, S.T.; Wimmers, A.J.; Pavolonis, M.; Berendes, T.A.; Haggerty, J.; et al. Aviation applications for satellite-based observations of cloud properties, convection initiation, in-flight icing, turbulence, and volcanic ash. *Bull. Am. Meteorol. Soc.* **2007**, *88*, 1589–1607. [CrossRef]
26. Slingo, A.; Slingo, J.M. The response of a general circulation model to cloud longwave forcing, Part 1: Introduction and initial experiments. *Q. J. R. Meteorol. Soc.* **1988**, *114*, 1027–1062. [CrossRef]
27. Baker, M.B. Cloud microphysics and climate. *Science* **1997**, *276*, 1072–1078. [CrossRef]
28. Niemelä, S.; Räisänen, P.; Savijärvi, H. Comparison of surface radiative flux parameterizations—Part I: Longwave radiation. *Atmos. Res.* **2001**, *58*, 1–18. [CrossRef]
29. An, N.; Pinker, R.T.; Wang, K.; Rogers, E.; Zuo, Z. Evaluation of cloud base height in the North American Regional Reanalysis using ceilometer observations. *Int. J. Climatol.* **2020**, *40*, 3161–3178. [CrossRef]
30. Pandey, P.C.; Njoku, E.G.; Waters, J.W. Inference of cloud temperature and thickness by microwave radiometry from space. *J. Climatol. Appl. Meteorol.* **1983**, *22*, 1894–1898. [CrossRef]
31. Liu, G.; Curry, J.A.; Sheu, R.-S. Classification of clouds over the western equatorial Pacific Ocean using combined infrared and microwave satellite data. *J. Geophys. Res.* **1995**, *100*, 13811–13826. [CrossRef]
32. Wilheit, T.T.; Hutchison, K.D. Retrieval of Cloud base heights from passive microwave and cloud top temperature data. *IEEE Trans. Geosci. Remote Sens.* **2000**, *38*, 1253–1259. [CrossRef]
33. Kokhanovsky, A.A.; Rozanov, V.V. Cloud bottom altitude determination from a satellite. *IEEE Trans. Geosci. Remote Sens. Lett.* **2005**, *2*, 280–283. [CrossRef]
34. Ferlay, N.; Thieuleux, F.; Cornet, C.; Davis, A.B.; Dubuisson, P.; Ducos, F.; Parol, F.; Riédi, J.; Vanbauce, C. Toward new inferences about cloud structures from multidirectional measurements in the oxygen A band: Middle-of-cloud pressure and cloud geometrical thickness from POLDER3/PARASOL. *J. Appl. Meteorol. Climatol.* **2010**, *49*, 2492–2507. [CrossRef]
35. Lelli, L.; Weber, M.; Burrows, J.P. Evaluation of SCIAMACHY ESA/DLR Cloud Parameters Version 5.02 by Comparisons to Ground-Based and Other Satellite Data. *Front. Environ. Sci.* **2016**, *4*, 43. [CrossRef]
36. Richardson, M.; Leinonen, J.; Cronk, H.Q.; McDuffie, J.; Lebsock, M.D.; Stephens, G.L. Marine liquid cloud geometric thickness retrieved from OCO-2′s oxygen A-band spectrometer. *Atmos. Meas. Tech.* **2019**, *12*, 1717–1737. [CrossRef]
37. Barker, H.W.; Jerg, M.P.; Wehr, T.; Kato, S.; Donovan, D.P.; Hogan, R.J. A 3D cloud-construction algorithm for the EarthCARE satellite mission. *Q. J. R. Meteorol. Soc.* **2011**, *137*, 1042–1058. [CrossRef]
38. Sun, X.J.; Li, H.R.; Barker, H.W.; Zhang, R.W.; Zhou, Y.B.; Liu, L. Satellite-based estimation of cloud-base heights using constrained spectral radiance matching. *Q. J. R. Meteorol. Soc.* **2016**, *142*, 224–232. [CrossRef]
39. Hutchison, K.D. The retrieval of cloud base heights from MODIS and three-dimensional cloud fields from NASA's EOS Aqua mission. *Int. J. Remote Sens.* **2002**, *23*, 5249–5265. [CrossRef]
40. Hutchison, K.D.; Wong, E.; Ou, S.C. Cloud base height retrieval during nighttime conditions with MODIS data. *Int. J. Remote Sens.* **2006**, *27*, 2847–2862. [CrossRef]
41. Minnis, P.; Sun-Mack, S.; Young, D.F.; Heck, P.W.; Garber, D.P.; Chen, Y.; Spangenberg, D.A.; Arduini, R.F.; Trepte, Q.Z.; Smith, W.L.; et al. CERES edition-2 cloud property retrievals using TRMM VIRS and Terra and Aqua MODIS data—Part I: Algorithms. *IEEE Trans. Geosci. Remote Sens.* **2011**, *49*, 4374–4400. [CrossRef]
42. Herzegh, P.; Wiener, G.; Bateman, R.; Cowie, J.; Black, J. Data fusion enables better recognition of ceiling and visibility hazards in aviation. *Bull. Am. Meteorol. Soc.* **2015**, *96*, 526–532. [CrossRef]
43. Bankert, R.L.; Hadjimichael, M.; Kuciauskas, A.P.; Thompson, W.T.; Richardson, K. Remote cloud ceiling assessment using data mining methods. *J. Appl. Meteorol.* **2004**, *43*, 1929–1946. [CrossRef]
44. Brenguier, J.L.; Pawlowska, H.; Schüller, L.; Preusker, R.; Fischer, J.; Fouquart, Y. Radiative properties of boundary layer clouds: Droplet effective radius versus number concentration. *J. Atmos. Sci.* **2000**, *57*, 803–821. [CrossRef]
45. Bendix, J.; Thies, B.; Cermak, J.; Nauß, T. Ground fog detection from space based on MODIS daytime data—A feasibility study. *Weather Forecast.* **2005**, *20*, 989–1005. [CrossRef]
46. Meerkötter, R.; Bugliaro, L. Diurnal evolution of cloud base heights in convective cloud fields from MSG/SEVIRI data. *Atmos. Chem. Phys.* **2009**, *9*, 1767–1778. [CrossRef]
47. Tan, Z.; Huo, J.; Ma, S.; Han, D.; Wang, X.; Hu, S.; Yan, W. Estimating cloud base height from Himawari-8 based on a random forest algorithm. *Int. J. Remote Sens.* **2021**, *42*, 2485–2501. [CrossRef]
48. Lewis, H.; Bowyer, J.; Broad, A.L.; Chamberlain-Clay, A.; Jones, C.; Chan, S.; Kahraman, A.; Morcrette, C. Using machine learning to find cloud-base height: A didactic challenge. *Weather* **2022**. [CrossRef]
49. Seaman, C.J.; Noh, Y.J.; Miller, S.D.; Heidinger, A.K.; Lindsey, D.T. Cloud base height estimation from VIIRS. Part I: Operational algorithm validation against CloudSat. *J. Atmos. Ocean. Technol.* **2017**, *34*, 567–583. [CrossRef]
50. Noh, Y.J.; Forsythe, J.M.; Miller, S.D.; Seaman, C.J.; Li, Y.; Heidinger, A.K.; Lindsey, D.T.; Rogers, M.A.; Partain, P.T. Cloud base height estimation from VIIRS. Part II: A statistical algorithm based on A-Train satellite data. *J. Atmos. Ocean. Technol.* **2017**, *34*, 585–598. [CrossRef]
51. Winker, D.M.; Hunt, W.H.; McGill, M.J. Initial performance assessment of CALIOP. *Geophys. Res. Lett.* **2007**, *34*, L19803. [CrossRef]
52. Winker, D.M.; Vaughan, M.A.; Omar, A.H.; Hu, Y.; Powell, K.A.; Liu, Z.; Hunt, W.H.; Young, S.A. Overview of the CALIPSO mission and CALIOP data processing algorithms. *J. Atmos. Ocean. Technol.* **2009**, *26*, 2310–2323. [CrossRef]

53. Stephens, G.L.; Vane, D.G.; Tanelli, S.; Im, E.; Durden, S.; Rokey, M.; Reinke, D.; Partain, P.; Mace, G.G.; Austin, R.; et al. CloudSat mission: Performance and early science after the first year of operation. *J. Geophys. Res.* **2008**, *113*, D00A18. [CrossRef]
54. Stephens, G.L.; Winker, D.; Pelon, J.; Trepte, C.; Vane, D.; Yuhas, C.; L'Ecuyer, T.; Lebsock, M. CloudSat and CALIPSO within the A-Train: Ten Years of Actively Observing the Earth System. *Bull. Am. Meteorol. Soc.* **2018**, *99*, 569–581. [CrossRef]
55. Heymsfield, A.J.; Winker, D.; van Zadelhoff, G.-J. Extinction-ice water content-effective radius algorithms for CALIPSO. *Geophys. Res. Lett.* **2005**, *32*, L10807. [CrossRef]
56. Austin, R.T.; Heymsfield, A.J.; Stephens, G.L. Retrieval of ice cloud microphysical parameters using the CloudSat millimeter-wave radar and temperature. *J. Geophys. Res.* **2009**, *114*, D00A23. [CrossRef]
57. Haynes, J.M.; Noh, Y.J.; Miller, S.D.; Haynes, K.D.; Ebert-Uphoff, I.; Heidinger, A. Low Cloud Detection in Multilayer Scenes using Satellite Imagery with Machine Learning Methods. *J. Atmos. Ocean. Technol.* **2021**, *39*, 319–334. [CrossRef]
58. Micke, K. Every pixel of GOES-17 imagery at your fingertips. *Bull. Am. Meteorol. Soc.* **2018**, *99*, 2217–2219. [CrossRef]
59. Miller, S.D.; Noh, Y.J.; Heidinger, A.K. Liquid-top mixed-phase cloud detection from shortwave-infrared satellite radiometer observations: A physical basis: Liquid-top mixed-phase cloud detection. *J. Geophys. Res.* **2014**, *119*, 8245–8267. [CrossRef]
60. Zhang, J.; Howard, K.; Langston, C.; Vasiloff, S.; Kaney, B.; Arthur, A.; Van Cooten, S.; Kelleher, K.; Kitzmiller, D.; Ding, F.; et al. National Mosaic and Multi-Sensor QPE (NMQ) system: Description, results, and future plans. *Bull. Am. Meteorol. Soc.* **2011**, *92*, 1321–1338. [CrossRef]
61. Nayak, M.; Witkowski, M.; Vane, D.; Livermore, T.; Rokey, M. CloudSat anomaly recovery and operational lessons learned. In Proceedings of the 12th International Conference on Space Operations (SpaceOps), Stockholm, Sweden, 11–15 June 2012; Paper 1295798. Available online: https://trs.jpl.nasa.gov/handle/2014/42598 (accessed on 26 August 2022). [CrossRef]
62. Miller, S.D.; Stephens, G.L. Multiple Scattering Effects in the Lidar Pulse Stretching Problem. *J. Geophys. Res.* **1999**, *104*, 22205–22219. [CrossRef]
63. Schiffer, R.A.; Rossow, W.B. The International Satellite Cloud Climatology Project (ISCCP): The First Project of the World Climate Research Programme. *Bull. Am. Meteorol. Soc.* **1983**, *64*, 779–784. [CrossRef]
64. Yuan, T.; Oreopoulos, L. On the global character of overlap between low and high clouds. *Geophys. Res. Lett.* **2013**, *40*, 5320–5326. [CrossRef]
65. Esmaili, R.; Nadia, S.; Schoeberl, M.; Barnet, C. Evaluating Satellite Sounding Temperature Observations for Cold Air Aloft Detection. *Atmosphere* **2020**, *11*, 1360. [CrossRef]
66. Weaver, G.M.; Smith, N.; Berndt, E.B.; White, K.D.; Dostalek, J.F.; Zavodsky, B.T. Addressing the Cold Air Aloft Aviation Challenge with Satellite Sounding Observations. *J. Oper. Meteorol.* **2019**, *7*, 138–152. [CrossRef]
67. Barnet, C.D.; Divakarla, M.; Gambacorta, A.; Iturbide-Sanchez, F.; Nalli, N.R.; Pryor, K.; Tan, C.; Wang, T.; Warner, J.; Zhang, K.; et al. *The NOAA Unique Combined Atmospheric Processing System (NUCAPS) Algorithm Theoretical Basis Document*; National Oceanic and Atmospheric Administration: Washington, DC, USA, 2021. Available online: https://www.star.nesdis.noaa.gov/jpss/documents/ATBD/ATBD_NUCAPS_v3.1.pdf (accessed on 25 August 2022).
68. Marder, J. New Data Product Warns Alaska Pilots of Clouds, Dangerously Cold Weather. NASA Online News "Benefits to You" Released on 19 August 2022. Available online: https://www.nasa.gov/feature/new-data-product-warns-alaska-pilots-of-clouds-dangerously-cold-weather (accessed on 25 August 2022).
69. Nakajima, T.; King, M.D. Determination of the optical thickness and effective particle radius of clouds from reflected solar radiation measurements—Part I: Theory. *J. Atmos. Sci.* **1990**, *47*, 1878–1893. [CrossRef]
70. Platnick, S.; King, M.D.; Ackerman, S.A.; Menzel, W.P.; Baum, B.A.; Riedi, J.C.; Frey, R.A. The MODIS cloud products: Algorithms and examples from Terra. *IEEE Trans. Geosci. Remote Sens.* **2003**, *41*, 459–473. [CrossRef]
71. Platnick, S.; Meyer, K.G.; King, M.D.; Wind, G.; Amarasinghe, N.; Marchant, B.; Arnold, G.T.; Zhang, Z.; Hubanks, P.A.; Holz, R.E.; et al. The MODIS cloud optical and microphysical products: Collection 6 updates and examples from Terra and Aqua. *IEEE Trans. Geosci. Remote Sens.* **2017**, *55*, 502–525. [CrossRef]
72. Walther, A.; Heidinger, A.K.; Miller, S.D. The expected performance of cloud optical and microphysical properties derived from Suomi NPP VIIRS day/night band lunar reflectance. *J. Geophys. Res.* **2013**, *118*, 13,230–13,240. [CrossRef]
73. Miller, S.D.; Straka, W.C., III; Mills, S.P.; Elvidge, C.D.; Lee, T.F.; Solbrig, J.E.; Walther, A.; Heidinger, A.K.; Weiss, S.C. Illuminating the Capabilities of the Suomi National Polar-Orbiting Partnership (NPP) Visible Infrared Imaging Radiometer Suite (VIIRS) Day/Night Band. *Remote Sens.* **2013**, *5*, 6717–6766. [CrossRef]
74. Miller, S.D.; Turner, R.E. A dynamic lunar spectral irradiance data set for NPOESS/VIIRS Day/Night Band nighttime environmental applications. *IEEE Trans. Geosci. Remote Sens.* **2009**, *47*, 2316–2329. [CrossRef]
75. Miller, S.D.; Mills, S.P.; Elvidge, C.D.; Lindsey, D.T.; Lee, T.F.; Hawkins, J.D. Suomi satellite brings to light a unique frontier of nighttime environmental sensing capabilities. *Proc. Natl. Acad. Sci. USA* **2012**, *109*, 15706–15711. [CrossRef]
76. Fukushima, K.; Miyake, S. Neocognitron: A new algorithm for pattern recognition tolerant of deformations and shifts in position. *Pattern Recognit.* **1982**, *15*, 455–469. [CrossRef]
77. Ronneberger, O.; Fischer, P.; Brox, T. U-Net: Convolutional Networks for Biomedical Image Segmentation. In *Medical Image Computing and Computer-Assisted Intervention—MICCAI 2015*; Navab, N., Hornegger, J., Wells, W., Frangi, A., Eds.; Lecture Notes in Computer Science; Springer: Cham, Switzerland, 2015; Volume 9351, pp. 234–241. [CrossRef]

78. Boukabara, S.-A.; Garrett, K.; Chen, W.; Iturbide-Sanchez, F.; Grassotti, C.; Kongoli, C.; Chen, R.; Liu, Q.; Yan, B.; Weng, F.; et al. MiRS: An all-weather 1DVAR satellite data assimilation and retrieval system. *IEEE Trans. Geosci. Remote Sens.* **2011**, *49*, 3249–3272. [CrossRef]
79. Ferraro, R.; Meyers, P.; Chang, P.; Jelenak, Z.; Grassotti, C.; Liu, S.Y. Application of GCOM-W AMSR2 and S-NPP ATMS hydrological products to a flooding event in the United States. *IEEE J. Sel. Top. Appl. Earth Obs. Remote Sens.* **2017**, *10*, 3884–3891. [CrossRef]
80. Breiman, L. Random forests. *Mach. Learn.* **2001**, *45*, 5–32. [CrossRef]
81. Illingworth, A.J.; Barker, H.W.; Beljaars, A.; Ceccaldi, M.; Chepfer, H.; Clerbaux, N.; Cole, J.; Delanoë, J.; Domènech, C.; Donovan, D.P.; et al. The EarthCARE Satellite: The next step forward in global measurements of clouds aerosols precipitation and radiation. *Bull. Am. Meteorol. Soc.* **2015**, *96*, 1311–1332. [CrossRef]
82. Hou, A.Y.; Kakar, R.K.; Neeck, S.; Azarbarzin, A.A.; Kumerrow, C.D.; Kojima, M.; Oki, R.; Nakamura, K.; Iguchi, T. The Global Precipitation Measurement mission. *Bull. Am. Meteorol. Soc.* **2014**, *95*, 701–722. [CrossRef]